The Nonlinear Evolution of Barotropically Unstable Jets

F. J. POULIN

Department of Mathematics, Massachusetts Institute of Technology, Cambridge, Massachusetts

G. R. FLIERL

Department of Earth, Atmospheric and Planetary Sciences, Massachusetts Institute of Technology, Cambridge, Massachusetts

(Manuscript received 26 November 2001, in final form 10 March 2003)

ABSTRACT

The instability of jets in the context of the shallow-water model for both quasigeostrophic (QG) and non-QG parameters is studied. First, the linear stability problem is solved for a wide range of Rossby and Froude numbers to elucidate the functional dependency of growth rate on these two nondimensional parameters. Then the nonlinear evolution of the instability is investigated through the use of numerical experiments. The QG scenarios produce a vortex street with cyclones and anticyclones that are symmetric in size, strength, and shape, as predicted by QG. In the non-QG regime the instability yields cyclones and anticyclones that can be asymmetric in all three properties. The authors comment on some interesting connections this work has with the Denmark Strait overflow.

1. Introduction

Vortices are of extreme importance in geophysical fluid dynamics since they act to transport physical, chemical, and biological properties throughout the world's atmosphere and oceans. It is the rapid rotation of the vortices that inhibits mixing between the interior and the ambient water and gives them a slow decay rate on relatively long timescales in comparison to their rotation rates (Armi and Zenk 1984; Wunsch 1984; Flierl et al. 1999). There are many different mechanisms by which eddies are created. One is through the instability of large-scale currents such as the Gulf Stream, the North Atlantic Current, the Azores Current, and the Agulhas Current. The coherent eddies produced by these jets transport fluid with anomalous temperature and salinity over large distances giving a significant contribution to the oceans thermohaline circulation (Wunsch 1984). The instability of these jets has often been modeled using quasigeostrophy (QG) since they typically have small Rossby numbers. However, these and other currents can sometimes have larger Rossby numbers than is beyond the scope of QG.

To accurately model these coastal jets requires including the rotation of the earth and the stratification of the fluid. However, it has been remarked by Vallis (1996) that a vertical expansion of the primitive equations in isentropic coordinates yields that each mode satisfies equations similar to the shallow-water (SW) equations. Therefore, before one attempts to study these jets in the context of the primitive equations, one should understand this simpler one-layer problem. In this article we explore the dynamics of jets in the SW model in a broader parameter space than what has been done to date.

There are many different intermediate models that lie in the range between QG and SW theory. Over a decade ago, a series of studies were performed to determine the strengths and weaknesses of these models (Allen et al. 1990a,b; Barth et al. 1990). Since this work, the increase in speed of computer processors has made it quite feasible to solve the SW equations directly, rather than resorting to using intermediate models. This is why we feel that in order to best understand the nonlinear dynamics of jets and eddies, in a parameter regime where the validity of these intermediate models may break down, one should solve the full SW equations.

The original focus of Allen et al. (1990a,b) and Barth et al. (1990) was to study jets and eddies that flow over continental shelves or slopes. Typically, these flows have order-1 Rossby numbers and deformations in the layer on the same order as the mean depth of the layer itself. Some excellent examples of such flows are dense water flows over sills at the Denmark Strait overflow (DSO) and the Strait of Gibraltar overflow (SGO) from the Mediterranean. These flows can have Rossby numbers close to 1 and 0.5, respectively, which is why one cannot expect QG to describe their dynamics. These

Corresponding author address: Francis Poulin, Scripps Institution of Oceanology, Mail Code 0218, UCSD, 9500 Gilman Drive, La Jolla, CA 92093-0218.
E-mail: fjpoulin@alum.mit.edu

currents are of fundamental importance in that they introduce anomalous vorticity, temperature, salinity, and possibly even nutrients into the ambient waters (Spall and Price 1998).

The DSO and SGO are similar in many ways, but the DSO is special in that the mooring data and hydrographic properties indicate that it has a much higher mesoscale variability than other straits (Spall and Price 1998; Jungclaus et al. 2001). Close to the sill both cyclones and anticyclones are generated. The former grow to be stronger because of cyclogenesis whereby the vortex tubes are predominantly stretched. Therefore, these intense mesoscale cyclones are generated in an environment of order-1 Rossby number. In contrast, the SGO has weaker variability and observations indicate that there are a predominance of anticyclones (also known as meddies) that are generated (Jungclaus 1999; Prater and Sanford 1994). Jungclaus et al. (2001) argued that the behavior of the jet is dependent on the value of the Rossby number. We agree with this hypothesis but emphasize that it is not sufficient to consider only this parameter. Indeed, in this article we will present two jets of equal Rossby number but different Froude numbers, which give rise to different structures. This leads us to believe that it is a combination of Rossby and Froude numbers that generate the different mesoscale variability and subsequently the different structures.

The study of strongly nonlinear jets forced by the underlying topography is complicated. Therefore, as a first step we study the dynamics of such flows over flat bottoms, a question that is of interest in its own right. This way we can better understand the properties of the current by itself and then later, one could consider the more difficult problem of the current overlying uneven topography. We note that the results of Jungclaus (1999) are independent of whether there is uneven topography, which suggests that this might not be essential in generating the instability.

Second, inspired by analysis aforementioned by Vallis (1996), we will neglect stratification by focusing on a reduced-gravity model. There have been many attempts to study these flows using two layers or even continuous stratification (Swaters and Flierl 1991; Swaters 1991; Karsten et al. 1995; Poulin and Swaters 1999a,b; Reszka et al. 2002). To model these flows accurately one would certainly want to include stratification and topography. However, our goal is not to study any particular jet, but instead, we want to focus on the basic mechanisms at work.

In the dense overflow context, the eddies we study fall into the category of submesoscale coherent vortices (McWilliams 1985). We focus on oceanographic situations but remark that there are similar scenarios in the atmosphere where non-QG flows generate vortices. For instance, ageostrophic vortices are generated by such phenomena as hurricanes, tornadoes, and mesoscale storms. An example of how unstable jets can form weather patterns in the atmosphere can be found in Schär and Davies (1990).

The barotropic instability of jets in QG was studied extensively in Flierl et al. (1987). They demonstrated that, when cyclones and anticyclones were generated, they are symmetric in their size, strength, and shape: they only differ in polarity. This artificial symmetry is imposed by the fact that geostrophic balance holds to leading order. To explore what asymmetries arise in non-QG regimes, we study the instability of a jet in the SW model. This system is richer than QG since it allows for large deformations in height, variable rotation rates, and the centrifugal forces to appear in the leading order balance. By increasing the size of the free surface deformations, we discover that asymmetries develop in all three properties.

The asymmetries between vortices in the SW model have already been studied to some extent. Cyclone–anticyclone asymmetry was addressed in Stegner and Dritschel (2000) where it was determined that ageostrophic effects stabilized cyclones and destabilized anticyclones. It was shown that large Froude numbers always stabilized the eddies. Polvani et al. (1994) and Arai and Yamagata (1994) studied two-dimensional SW turbulence and observed asymmetries between the evolution of interacting vortices; anticyclones are favored and merge to take coherent circular forms. In contrast, the cyclones become elongated because of the enstrophy cascade. Baey et al. (1999) studied the instability of a two-layer SW jet that allowed for baroclinic instability. However, they did not consider Rossby numbers larger than 0.3, which is why they did not notice the same asymmetries that we present in this work.

In section 2 we discuss the SW model and the numerical method used in our simulations. The following section describes the linear stability analysis of the geostrophic jets to illustrate the functional dependency of the growth rates and the length scale of the most unstable mode on the Rossby and Froude numbers. It is in section 4 that we present the numerical simulations and see the asymmetries that arise in the instability processes. Last, we summarize our findings and state important questions to be addressed in future work.

2. The model

We study a reduced-gravity model, also known as a $1\frac{1}{2}$-layer model, which consists of an active layer underlying or overlying an infinitely deep passive layer. Without loss of generality, we shall assume that the passive layer is situated above the active layer. The case where a motionless layer is above or below the dynamic layer can be used to idealize bottom dwelling or surface dwelling currents, respectively. Some examples of the former are regularly observed in the Strait of Georgia, the Denmark Strait overflow, and the Middle Atlantic Bight. Examples of the latter arise in the Gulf Stream,

the North Atlantic Current, the Azores Current, and the Agulhas Current.

a. Shallow-water equations

The inviscid, reduced-gravity, SW model in dimensional form is governed by the following system of partial differential equations:

$$\frac{\partial \mathbf{u}}{\partial t} + \mathbf{u} \cdot \boldsymbol{\nabla}\mathbf{u} + f\mathbf{k} \times \mathbf{u} = -g'\boldsymbol{\nabla}h \tag{1}$$

$$\frac{\partial h}{\partial t} + \boldsymbol{\nabla} \cdot (h\mathbf{u}) = 0. \tag{2}$$

The two parameters, g' and f, are the reduced gravity and the Coriolis parameter, both of which we assume to be constant. The variables $\mathbf{u} = (u, v)$ and h denote the horizontal velocity field and layer thickness, respectively. From these we define H as the mean layer thickness so that $\eta = h - H$ is the free surface deformation. In addition, L and U are the scales of the horizontal motion and velocity based on the width and peak velocity of the jet.

The two conventional nondimensional parameters are the Rossby number $\mathrm{Ro} = U/(fL)$ and rotational Froude number $\mathrm{Fr} = (fL)^2/(g'H)$. Solving the problem numerically requires friction for stability; the dimensional friction parameter is ν. This introduces a third parameter, a numerical Reynolds number $\mathrm{Re} = UL/\nu$.

b. Asymmetry between cyclones and anticyclones

To begin our discussion on asymmetry, let us first consider the potential vorticity (PV) of the SW model. Nondimensionalized, it is

$$\frac{\mathrm{Ro}\boldsymbol{\nabla} \times \mathbf{u} + 1}{1 + \mathrm{RoFr}\eta}. \tag{3}$$

The special case where $\mathrm{Ro} \ll 1$ and $\mathrm{Fr} = O(1)$ allows us to Taylor-expand the SW equations about $\mathrm{Ro} = 0$. The resulting model is what is referred to as QG. The governing equation is simply the statement that the QG PV

$$\nabla^2\eta - \mathrm{Fr}\eta \tag{4}$$

is conserved along trajectories of fluid parcels. This means that, as the relative vorticity increases (decreases) there must be a corresponding vertical stretching (contraction) of the vortex tubes (Pedlosky 1987). To derive QG it is necessary to assume that there are no order-one variations in the layer thickness in comparison to the mean thickness; this is in contrast to the SW model that can have order-one deformations. Interestingly, this varition of depth with the across-channel coordinate sets the horizontal scale of a geostrophic vortex, the radius of deformation,

$$L_R = \sqrt{g'H}/f, \tag{5}$$

which clearly increases with increasing depth. Since anticyclones and cyclones are generated in deep and SW respectively, the anticyclones tend to be wider. This has been observed in SW turbulence simulations of Polvani et al. (1994). We will demonstrate that this is also true in the formation of vortices through the instability of a jet.

Another assumption needed to derive QG is that the velocity is geostrophic to leading order. The SW model allows for eddies that exhibit gradient-wind balance:

$$\frac{v^2}{r} + fv = g'\frac{\partial h}{\partial r}. \tag{6}$$

Olson (1991) showed that in this balance relation the quadratic appearance of velocity does not permit arbitrarily strong negative pressure gradients. Hence there is a cutoff past which anticyclones cannot exist. Then the right-hand side cannot be arbitrarily large and negative since the left-hand side has a minimum negative value because of its quadratic structure. This is why for large Rossby number flows there is a preference for strong cyclones in atmospheric phenomenon such as mesoscale storms.

Another argument that shows this cyclone–anticyclone asymmetry stems from the criteria for inertial (centrifugal) stability, which states that the total vorticity is positive (Holton 1992). This prevents the formation of arbitrarily strong anticyclones since they violate this criteria. We remark that inertial instability produces three-dimensional and nonhydrostatic dynamics, something that is not permitted in the context of SW theory.

c. Numerical method to solve the SW model

We study the nonlinear evolution of a jet by numerically integrating the inviscid SW equations expressed in terms of the momentum transport functions, $\mathcal{U} = uh$ and $\mathcal{V} = vh$. This form is preferred since the nonlinearities are in conservation form. The equations are as follows:

$$\frac{\partial \mathcal{U}}{\partial t} + \frac{\partial}{\partial x}\left(\frac{\mathcal{U}^2}{h} + \frac{g'h^2}{2}\right) + \frac{\partial}{\partial y}\left(\frac{\mathcal{U}\mathcal{V}}{h}\right) = f\mathcal{V} \tag{7}$$

$$\frac{\partial \mathcal{V}}{\partial t} + \frac{\partial}{\partial x}\left(\frac{\mathcal{U}\mathcal{V}}{h}\right) + \frac{\partial}{\partial y}\left(\frac{\mathcal{V}^2}{h} + \frac{g'h^2}{2}\right) = -f\mathcal{U} \tag{8}$$

$$\frac{\partial h}{\partial t} + \frac{\partial \mathcal{U}}{\partial x} + \frac{\partial \mathcal{V}}{\partial y} = 0. \tag{9}$$

The geometry we consider is that of a channel where the across and along-channel coordinates are x and y respectively. We assume that there are rigid boundaries at $x = \pm 1$ and that the channel is periodic so that $y = \pm 1$ coincide. The flat bottom is located at $z = 0$, the free surface is denoted by η, and therefore the total depth is $h = 1 + \eta$ since the mean depth is 1.

The equations are solved on an unstaggered grid with

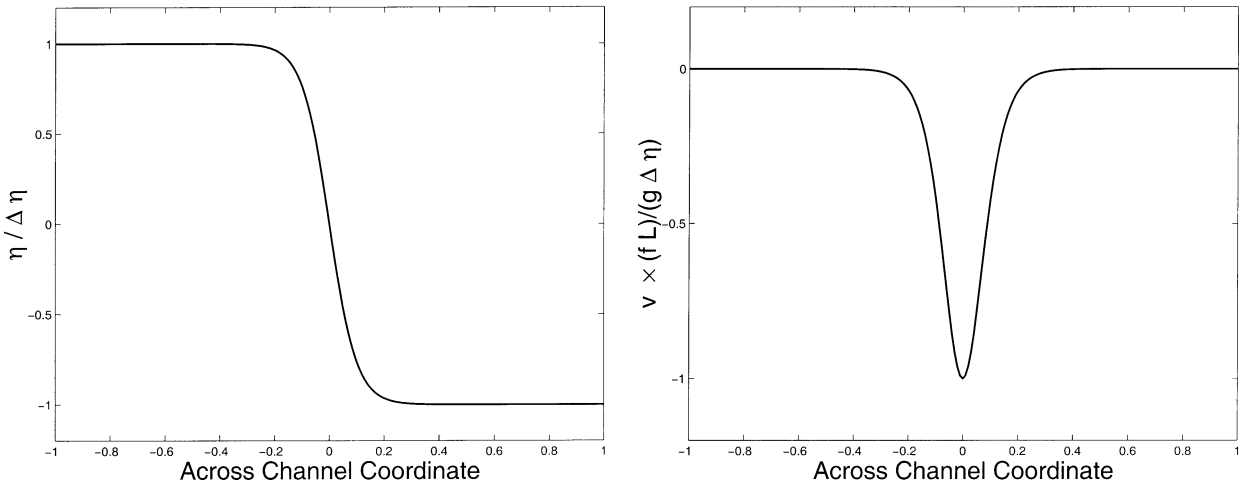

FIG. 1. The plots are the (left) free surface and (right) velocity fields of the basic-state profiles investigated; they are defined in (11) and (13).

a finite-difference scheme. The advection and pressure terms are discretized by third-order upwinding (downwinding) and fourth-order center differencing schemes, respectively. The equations are evolved forward in time by the third-order Adams–Bashford method [see Fletcher (1991)]. The square domain is a 200 × 200 regular grid and the state variables are defined at each node of the grid. We have verified the results of particular non-QG simulations by doing similar calculations on a 400 × 400 grid to ensure these results are robust.

In order to guarantee numerical stability, two measures were taken. The time step was chosen so that the Courant–Friedrichs–Lewy condition was satisfied:

$$\Delta t < \frac{\Delta x}{|u| + \sqrt{g'H}}. \tag{10}$$

As well, numerical friction was introduced into the momentum transport equations and the continuity equation as a Laplacian operator with a viscosity coefficient of ν. The numerical Reynolds number is on the order of 10^3 or higher. This term is included purely for the sake of maintaining numerical stability. Often when one uses spectral methods, one applies a hyperviscosity of the form $\nu(-1)^{n+1}\nabla^{2n}$ for some integer value of n. The reason is not because of any physical reasons but because it can establish numerical stability. Applying this type of diffusion is more problematic in finite-difference methods because of the large stencil it requires. For certain simulations we have decreased and increased the Reynolds number by a factor of 10 and have found that, though the simulations may vary slightly, their qualitative behavior persists. Thus we do not believe that the introduction of friction alters the qualitative behavior of the instability.

The boundary conditions are no-normal flow, free slip, and $\partial\eta/\partial x = 0$ in the x direction, and periodic boundary conditions in the y direction. We have chosen free slip instead of no slip because our grid is not fine enough to resolve the boundary layers that may develop. Even though the no-slip condition is valid at the microscopic scales, there is no reason to believe that it is the appropriate one when describing large-scale fluid dynamics, like the ones that we are interested in (Pedlosky 1996).

This numerical code is used with two objectives in mind. First, we compare the growth rates from the simulations to those predicted by the linear stability analysis in order to determine whether linear theory predicts the initial developments of the instability. Second, we study parameter choices in the non-QG regime to better understand what asymmetries may arise between cyclones and anticyclones. We consider mainly monochromatic perturbations containing only one wavelength in the along-channel direction, not because the physical world behaves in this simple manner but because it presents a cleaner picture of the instability processes. It illustrates what asymmetries develop in the absence of complicated vortex interactions.

d. Basic state

We take the jet to be a geostrophic Bickley jet (see Fig. 1):

$$\overline{\eta} = -\Delta\eta \tanh\left(\frac{x}{L}\right) \tag{11}$$

$$\overline{u} = 0 \tag{12}$$

$$\overline{v} = -\frac{g'\Delta\eta}{fL} \operatorname{sech}^2\left(\frac{x}{L}\right). \tag{13}$$

Note that the fluid is deeper in the left portion of the channel. The parameter $\Delta\eta$ denotes the maximum amplitude of the surface deformations from the mean and L is the length scale of the width of the jet. In the presence of viscosity the geostrophic state is no longer

an exact solution; however, since the friction coefficient is very small, the geostrophic state is a very good approximate solution.

We have also tried a similar profile where the velocity profile is Gaussian and the surface deformation is an error function. The results vary slightly in magnitude but yield the same qualitative results as presented in this article. This suggests that our qualitative results apply to any jet that is similar to the one under investigation. We shall present some examples of the instability of Gaussian profiles to demonstrate the similarity between the two.

In our simulations, $L = 1/10$ and $f = 10$. Therefore, the Rossby and Froude numbers simplify to $\mathrm{Ro} = U = \Delta\eta/\mathrm{Fr}$ and $\mathrm{Fr} = 1/g'$ and their product is equal to the amplitude of the surface variations $\Delta\eta$.

3. Linear stability analysis

a. Ripa's theorem

Two criteria are derived in Ripa (1983) that together are sufficient to guarantee the linear stability of a purely zonal flow in a reduced-gravity SW model on a β plane; they are referred to as Ripa's theorem. A weak version of Ripa's theorem, customized to flows with $\overline{u} = 0$ and $\overline{v}$ semidefinite in sign, states that the flow will be stable when

$$\frac{d}{dx}\left(\frac{\overline{v}_x + f}{H}\right) \neq 0 \quad \text{and} \tag{14}$$

$$|\overline{v}| \leq \sqrt{g'H}, \tag{15}$$

where H is the total depth of the basic state. The first criterion requires that the PV not possess local extrema. This is equivalent to the classical Rayleigh stability condition of QG dynamics (Pedlosky 1987) and is usually referred to as barotropic (shear) instability. The second criteria requires that the velocity at every point be bounded above by the surface gravity wave speed at that same point. In the QG limit, the surface gravity wave speed is in effect infinite, and therefore (15) is trivially satisfied. Ripa (1991) conjectured that, if only the first of these statements is violated, the PV gradient of the mean flow generates the instability and hence Rossby waves are produced. Conversely, if only the second condition is violated, the unstable modes that grow are inertio-gravity waves. This type of instability is called supersonic instability (Balmforth 1999; Takehiro and Hayashi 1992). In all of our simulations, (14) is violated and therefore Rossby waves are expected to develop. The second condition, (15), is satisfied for most of our simulations but is violated when $\Delta\eta$ is sufficiently large. Hence, highly non QG instabilities should contain both shear and supersonic instabilities. Ripa showed that inertial (centrifugal) instability cannot occur in a 1-layer SW model (Ripa 1983).

b. Linearized perturbation problem

Initially, the numerical simulations perturb the basic state with waves of amplitude at least two orders of magnitude smaller than the basic state itself, to insure that the initial dynamics are governed by the linearized equations. We use these equations to derive predictions of the growth rates in the linear regime and then compare them with those calculated from the numerical simulations.

In Flierl et al. (1987) it was determined that linear instability can indeed describe the initial process of growth for a barotropic QG jet. The linear stability problem in the SW model has been solved in various parameter regimes [see, e.g., Hayashi and Young (1987), Paldor and Ghil (1997), Balmforth (1999), Li and McClimans (2000), Stegner and Dritschel (2000), Baey et al. (1999)]. Unlike previous work, we design a method to solve the linear stability problem for the reduced-gravity SW equations for arbitrary Rossby and Froude numbers.

c. Method to solve the linear stability problem

The equations that govern the evolution of linear perturbations are obtained by first perturbing the basic state:

$$\begin{bmatrix} \eta \\ u \\ v \end{bmatrix} = \begin{bmatrix} \overline{\eta}(x) + \eta'(x, y, t) \\ u'(x, y, t) \\ \overline{v}(x) + v'(x, y, t) \end{bmatrix}. \tag{16}$$

The geostrophic solution depends only on the cross-channel coordinate, but we study its stability relative to two-dimensional perturbations. For our convenience, instead of linearizing the SW equations in transport form, those being the form we used in the numerical simulations, we linearize them in their canonical form, (1) and (2).

We substitute (16) into the SW equations and linearize to obtain the following linear equations:

$$\frac{\partial\eta'}{\partial t} + \frac{\partial(Hu')}{\partial x} + \overline{v}\frac{\partial\eta'}{\partial y} + H\frac{\partial v'}{\partial y} = 0 \tag{17}$$

$$\frac{\partial u'}{\partial t} + \overline{v}\frac{\partial u'}{\partial y} - fv' + g'\frac{\partial\eta'}{\partial x} = 0 \tag{18}$$

$$\frac{\partial v'}{\partial t} + \frac{d\overline{v}}{dx}u' + \overline{v}\frac{\partial v'}{\partial y} + fu' + g'\frac{\partial\eta'}{\partial y} = 0. \tag{19}$$

The perturbations are decomposed into a sum of normal-mode solutions, each of the form

$$\begin{bmatrix} \eta' \\ u' \\ v' \end{bmatrix} = \Re\left\{\begin{bmatrix} \hat{\eta}(x) \\ ik\hat{u}(x) \\ \hat{v}(x) \end{bmatrix} \exp[ik(y - ct)]\right\}. \tag{20}$$

The wavenumber and phase speed corresponding to motion in the y direction are denoted by k and c, respec-

tively; and the amplitude variables, $\hat{\eta}$, $\hat{u}$, and $\hat{v}$, are complex functions of x. The factor ik is incorporated into the decomposition for u' since the resulting system is real.

We determine the equations that govern the evolution of η', u', and v', by substituting (20) into (17) to (19), and then simplify to obtain

$$\begin{bmatrix} \overline{v} & \left(\frac{dH}{dx} + H\frac{d}{dx}\right) & H \\ -\frac{g'}{k^2}\frac{d}{dx} & \overline{v} & \frac{f}{k^2} \\ g' & \left(\frac{d\overline{v}}{dx} + f\right) & \overline{v} \end{bmatrix} \begin{bmatrix} \hat{\eta} \\ \hat{u} \\ \hat{v} \end{bmatrix} = c \begin{bmatrix} \hat{\eta} \\ \hat{u} \\ \hat{v} \end{bmatrix}. \quad (21)$$

This is the Rayleigh equation for the SW model for a one-dimensional geostrophic basic state (Pedlosky 1987). In (21) the phase speed is the eigenvalue of the differential matrix operator. Since we are unable to determine the eigenvalues of the matrix analytically, we apply a spectral collocation method to discretize the system (Trefethen 2000). The eigenvalues of this resulting system are then computed quite simply in MATLAB.

The boundary conditions are $\hat{u} = 0$ at $x = -1$ and $x = 1$. It was determined that, as the number of collocation points increased, the growth rates converged. There were spurious roots, as is typical of spectral schemes, but they did not have any positive growth rates and hence they did not affect our calculations. By using 200 collocation points we usually obtain convergence to within three significant digits.

d. Results of the linear analysis

A series of calculations was performed in order to determine the functional dependency of the most unstable wavenumber on the Rossby and Froude numbers. The perturbations were of the form $\sin(kx)$ with wavenumbers $k = \pi, 2\pi, 3\pi, 4\pi, 5\pi$, and 6π since they are the first six modes that fit in the channel and tended to be the most unstable. Figure 2 is a contour plot of the growth rate normalized by the Rossby number, which we refer to as the relative growth rate. For Froude numbers near the barotropic limit, Fr $\ll 1$, the relative growth rate is nearly independent of the Rossby number. For larger Froude numbers the relative growth rate decreases with increasing Rossby number, the effect of which is strengthened as the Froude number increases. It is clear that the QG model yields the largest relative growth rates with respect to the Rossby number. Moreover, the barotropic limit is always the most unstable, as found in the stability of vortices (Stegner and Dritschel 2000). This implies that the QG model overestimates the growth rates, as does the barotropic assumption. Therefore, the free surface acts as a stabilizing factor.

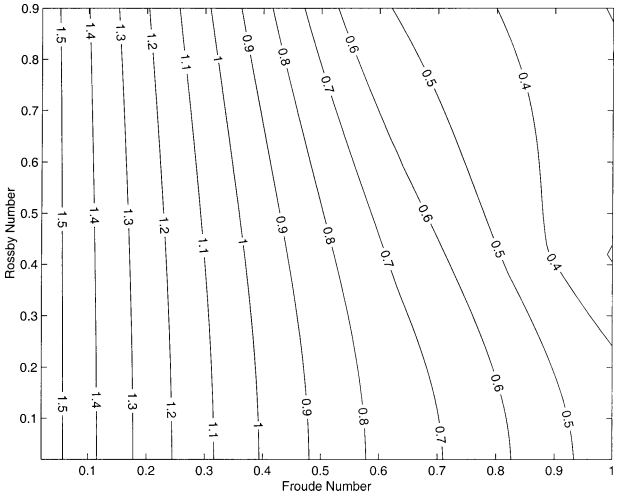

FIG. 2. A contour plot of the relative growth rate (growth rate/Ro) with respect to the two nondimensional parameters Ro $= U/(fL)$ and Fr $= (fL)^2/(g'H)$.

Some results of the numerical calculations are displayed in Fig. 3. The two plots in the top row present the relative growth rates for Fr $= 0.1$ and Fr $= 0.5$, respectively, and for various Rossby numbers, whereas the plots in the bottom row depict the relative growth rates for Ro $= 0.1$ and Ro $= 0.5$, respectively, for various Froude numbers. The top plots indicate that there is not any noticeable change in the wavelength of the most unstable mode: the most unstable mode is longer in the first case in comparison to the second. In contrast the bottom two plots illustrate how the most unstable mode moves to larger wavenumbers with increasing Froude number. These results all lead to the conclusion that an increase in Rossby number does not significantly affect the size of the most unstable mode, but that an increase of Froude number translates the most unstable mode to smaller scales.

4. Numerical simulations

In this section we present the results of the nonlinear evolution of a perturbed unstable jet, (11), (12), and (13), in the SW model for a select choice of parameters to explore cyclone–anticyclone asymmetry. Most of the simulations are monochromatic since that allows for a better comparison of the cyclones and anticyclones. The simulations with small Rossby number are essentially test cases since similar results have already been observed in QG simulations (Flierl et al. 1987). However, the cases of larger Rossby number explore new territory and illustrate what asymmetries are to be expected for various regions of parameter space.

Each plot consists of six snapshots of the relative vorticity for a particular simulation where the solid and dashed lines are positive and negative vortices, respec-

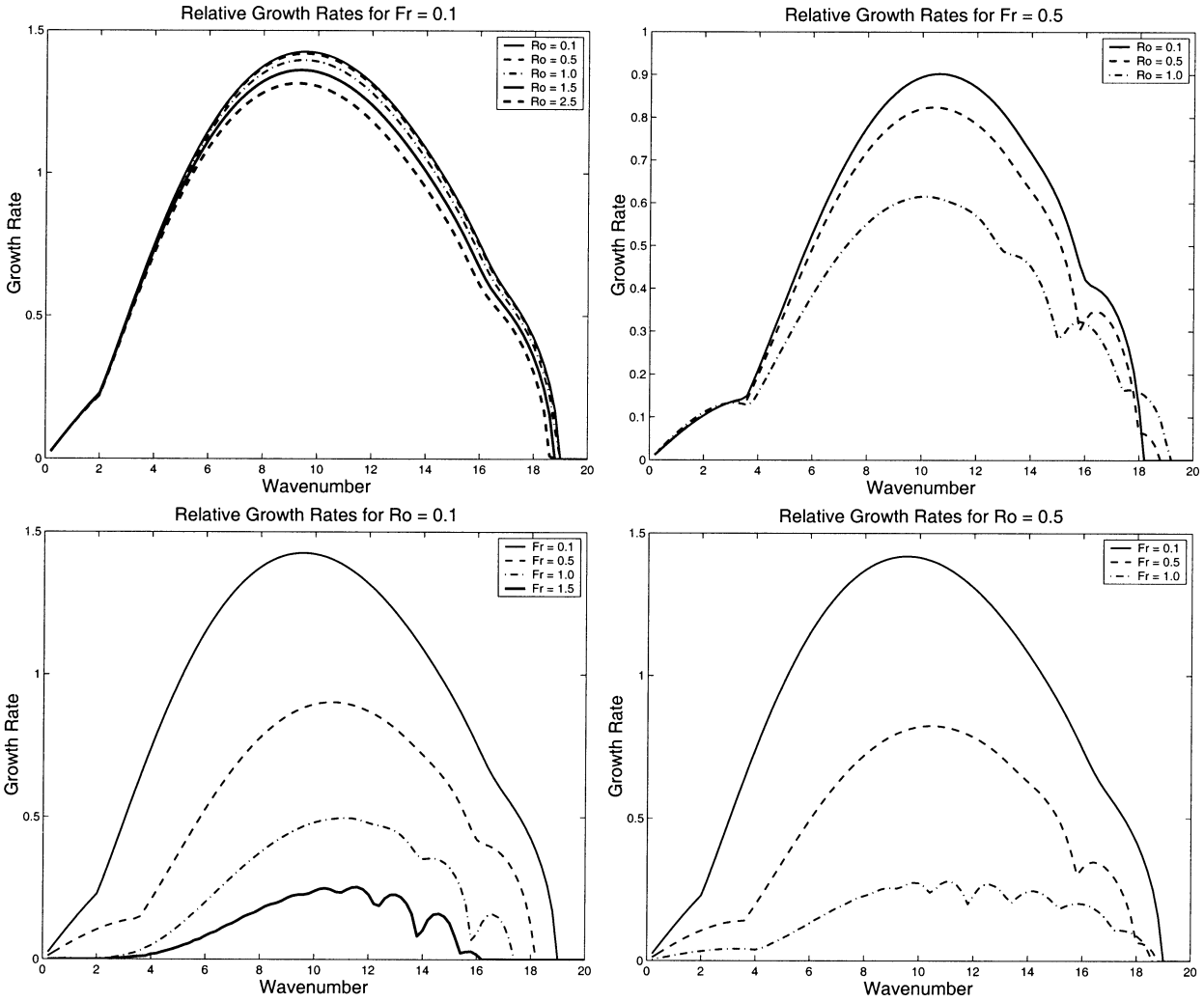

FIG. 3. Plots of the dependency of the relative growth rates on the Froude and Rossby numbers. They demonstrate that the most unstable wavenumber moves to slightly smaller scales as the Froude number increases. Also, changes in Rossby numbers have no obvious effect on the size of the most unstable mode.

tively, and the contour spacing is equal to Ro. The across-channel and along-channel coordinates correspond to the x and y axis, respectively. In all simulations the flow is down the page and the basic state is shallower on the right-hand side. For several cases we also plot the maximum of the cyclonic and anticyclonic vorticity as well as the position in the across-channel direction. These two combined indicate when the vortex tubes are stretched or contracted.

a. Ro = 0.1 and Fr = 0.1

Flows with parameters similar to these are quite common in the atmosphere and oceans. This is what makes QG a useful model since it accurately describes the dynamics of these currents. An example of a jet that is well situated in this regime is the North Atlantic Current (Baey et al. 1999). The QG model also has the advantage over the SW model in that it is more computationally inexpensive.

Figure 4 is very similar to the f-plane simulations in Flierl et al. (1987). The perturbations on the unstable jet grow in amplitude until the nonlinearities become significant, and the waves roll up and break. This nonlinear breaking generates vortices in the center, which form into a vortex street, but it also injects fluid across the jet that form dipoles. This injection is an important means through which fluid is transported between deep and shallow waters. The presence of dipoles reflects that transport has occurred. Typically, a more unstable jet will transport more fluid in comparison with a more stable one.

Until subharmonic instabilities develop (Saffman and Schatzman 1981), the vortices are symmetric in size, strength, and shape. There are two types of structures that are observed. The outer pools are the circular shapes

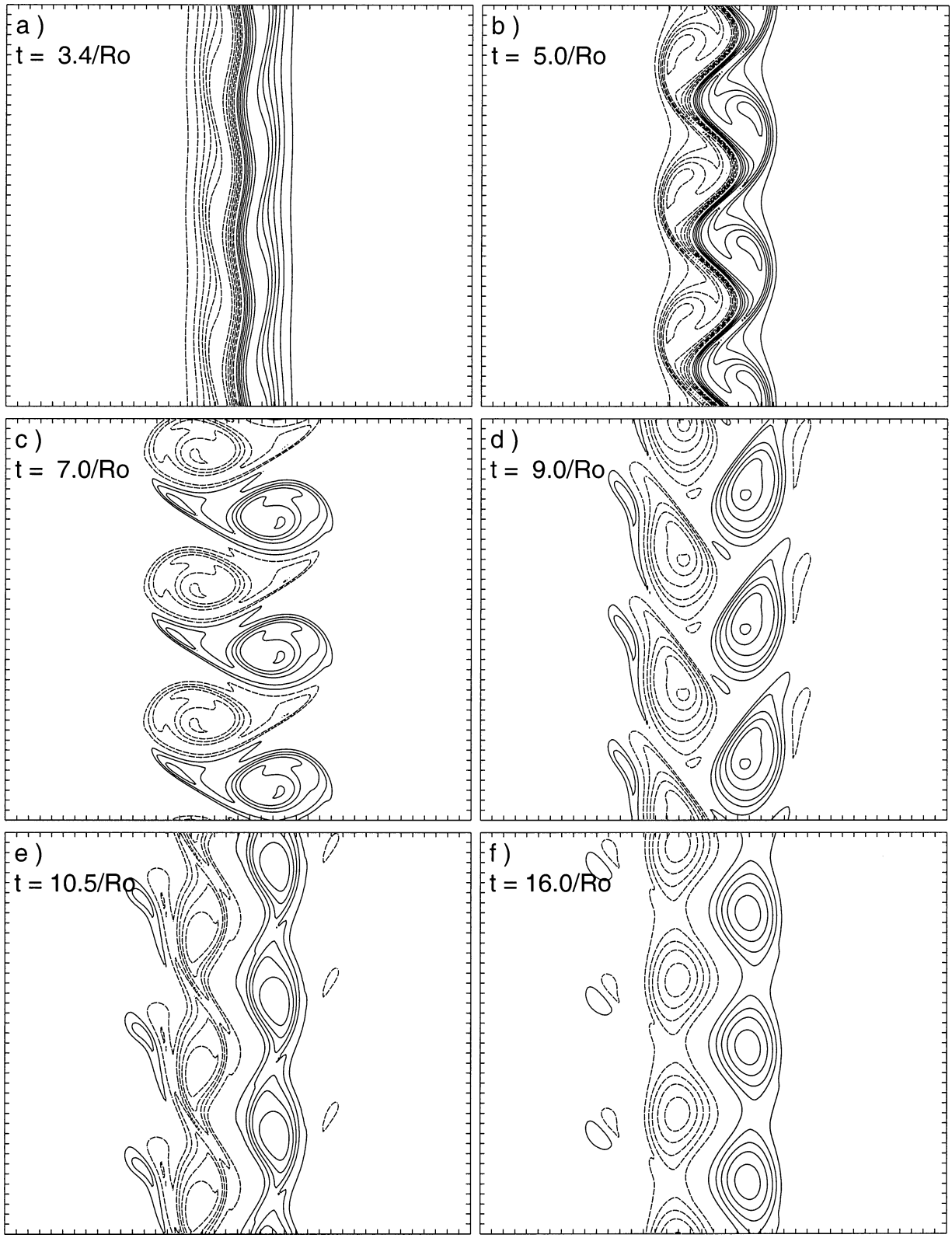

FIG. 4. Case for Ro = 0.1 and Fr = 0.1: this evolution is very similar to the f-plane simulations of Flierl et al. (1987).

that originate on the outskirts of the jet but then settle down to form the circular vortices in the vortex street. The inner pools form near the jet but are injected as filaments across the street.

b. Ro = 0.1 and Fr = 0.5

These flows are still well within the QG framework. However, the deformations from the mean of the layer thickness are larger than in the previous case, which makes QG theory slightly less accurate. A physical example that is close to this particular choice of parameters is the Azores Current (Baey et al. 1999).

Figure 5 presents snapshots of vorticity where free surface effects are more pronounced. In contrast to Fig. 4, the inner and outer pools do not pinch off and separate. Instead, the inner and outer pools merge to form a very compact triangular-shaped vortex street; this is usually referred to as a cat's-eye pattern (Drazin and Reid 1995). The similarity of this street to those obtained in Flierl et al. (1987) with a nonzero β parameter indicates that an increase in Froude number stabilizes the flow in a manner similar to an increase in the β parameter, as predicted from the linear theory. This stabilization prevents the injection of the inner pools and therefore strongly reduces, if not entirely eliminates, the transport of fluid across the jet. The transport of fluid across a jet due to barotropic instability is something that has been addressed in some detail in Rogerson et al. (1999).

Figure 6 plots the extrema of vorticity and their cross-channel positions versus time for these two aforementioned simulations. These curves track the strength and position of the outer pools since they are the strongest sources of vorticity. Initially, the vorticity decays, but then oscillations develop. This stretching and contracting of vortex tubes occurs because of the nearly periodic orbit of the peaks of the outer pools, which causes horizontal translation across the jet where the free surface is not uniform. This was observed in Flierl et al. (1987), and they explained that the oscillation is due to a transfer of energy between the mean flow and the perturbations. The amplitude of the oscillations are much weaker in Fig. 6a than in Fig. 6b because the deformation of the layer thickness is smaller. Consequently, the degree of symmetry appears to be reduced in Fig. 6b.

c. Ro = 1.0 and Fr = 0.1

The case of order-1 Rossby number is not typical throughout the oceanic interior but does often occur near coastlines where topography and friction become more important. We will show that in this region of parameter space there is a preference for producing stronger anticyclones. The laboratory experiments of Lane-Serff and Baines (1998) observed a similar type of asymmetry.

As in Fig. 4, both the cyclonic and anticyclonic fluids separate into inner and outer pools. The cyclonic outer pools reattach temporarily by Fig. 7e and then finally manage to achieve final separation by Fig. 7f. This reattachment is evidence that the cyclones are weaker than the anticyclones. The source of this asymmetry must come from the fact that the cyclones are generated in shallow water. The final frame shows that the anticyclonic outer pools are larger and stronger than the cyclones. The cyclones and anticyclones injected are relatively stronger than those in Fig. 4 which therefore generates stronger dipoles.

We have performed another numerical experiment for a similar jet where the velocity field is a Gaussian profile and the η field is the required error function that maintains the basic state in geostrophic balance. Not too surprising is that the vortices generated had the same qualitative behavior as described above. This suggests that all jets with similar velocity and free-surface profiles in this range of parameter space should exhibit the same behavior; the anticyclones produced from the instability are larger and stronger than the cyclones.

d. Ro = 1.0 and Fr = 0.5

In the DSO slightly past the sill, both the Rossby and Froude numbers are order 1 (L. Pratt 2001, personal communication). These combined factors are possibly the reason why it has a higher mesoscale variability than other overflows. Since the jet produces predominantly stronger cyclones, one might expect that this particular choice of parameters yields the same qualitative behavior. Indeed, this will be shown to be the case.

Figure 8 is the first simulation where the amplitude deformations are no longer small. Consequently, strongly non-QG instabilities arise. The anticyclonic fluid develops outer pools and relatively weak inner pools, as can be seen in the final frame. These inner pools do not pinch off as in Figs. 4 and 7, nor do they merge as in Fig. 5. Instead, they remain between the cyclonic outer pools on the edge of the front and a fixed distance from the center of the jet. They cannot be injected into the shallow waters since the cyclonic fluid does not leave any space for them to pass through, thereby impeding the fluid transport across the jet. Figure 8f illustrates that the cyclones are stronger then the anticyclones. The cyclones are unusual since they are boomerang shaped. The end result is a highly asymmetric vortex street where the cyclones and anticyclones possess completely different size, strengths, and shapes.

Figure 9a illustrates that the anticyclones are stronger than the cyclones. The cyclones travel in orbits that create oscillations in their amplitude. Since the centers are translated toward shallower waters, we have a net decrease in their strength. The anticyclones also travel in nearly periodic orbits but are shifted to deeper waters. This decreases the strength of the eddies but not as much as for the cyclones.

Conversely, Fig. 9b shows that cyclones are much

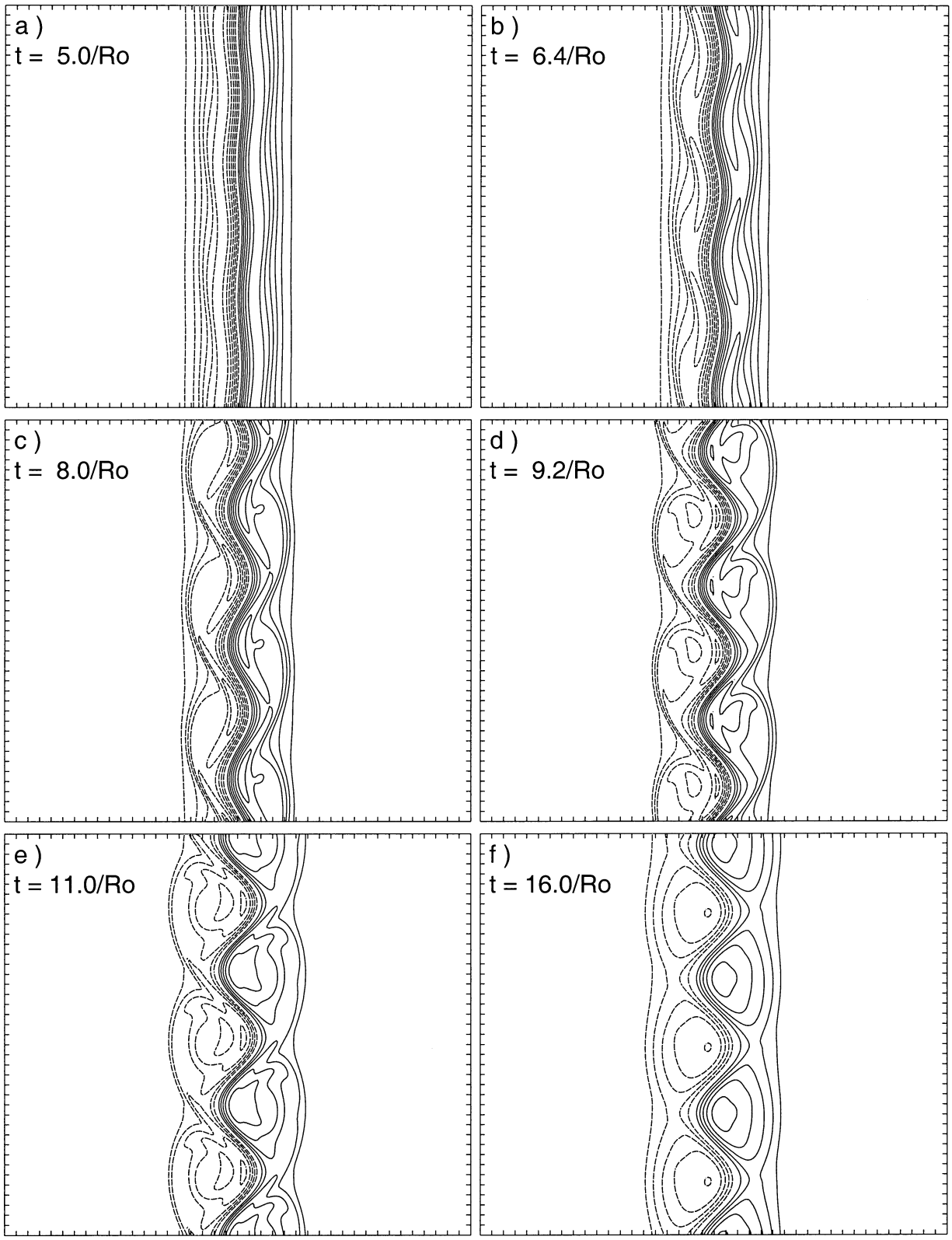

FIG. 5. Case for Ro = 0.1 and Fr = 0.5: the stabilizing effect of the Froude number is similar to that of the β plane since they both act to make vortices triangular in shape.

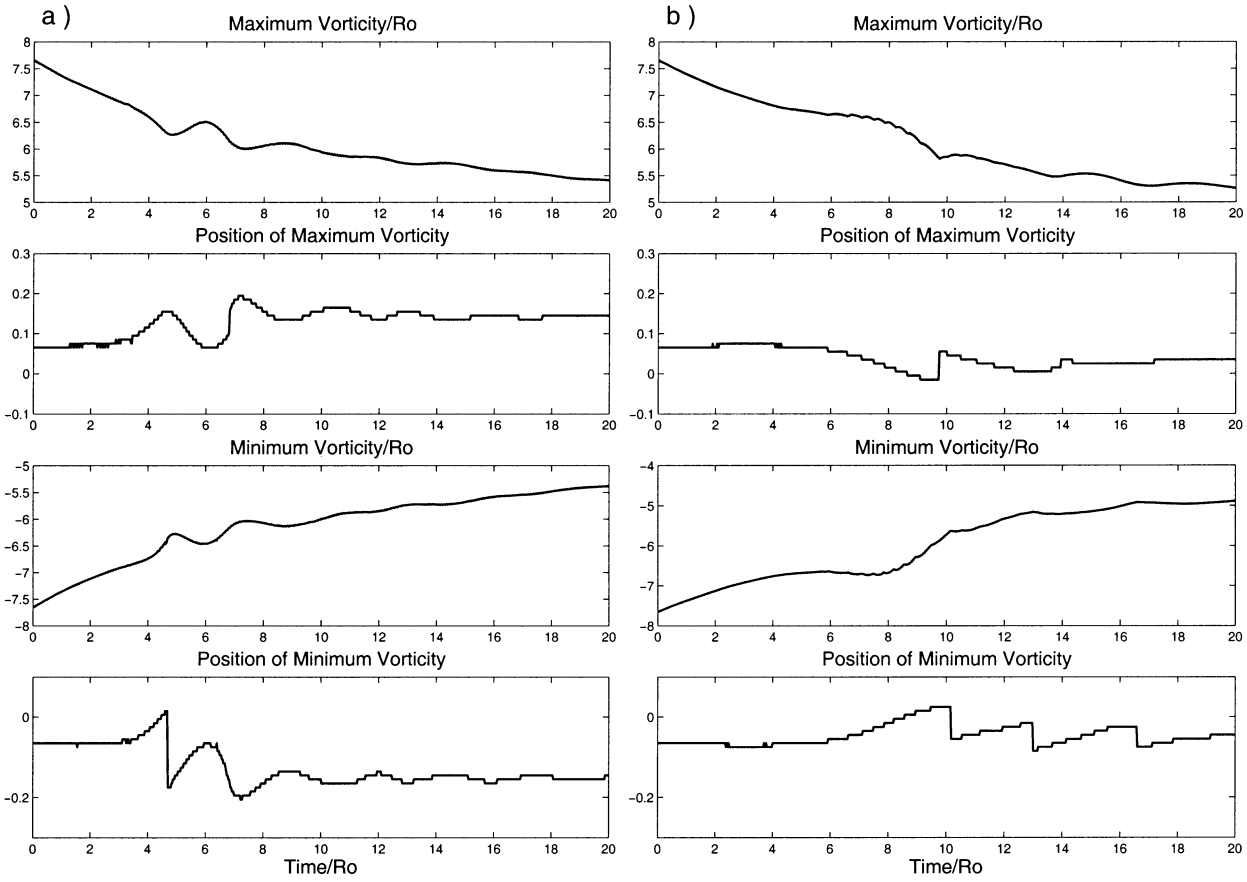

FIG. 6. Case for Ro = 0.1 and (a) Fr = 0.1 and (b) Fr = 0.5: These plots show that the value and position of the vorticity extrema are nearly symmetric. The oscillations that we observe are due to a transfer of energy between the mean flow and the perturbation field (Flierl et al. 1987).

stronger, the reason being that the street is translated into deeper water that stretches the vortex tubes, strengthening the cyclones and weakening the anticyclones. The process is not as clear as in Fig. 6 since the strong vortices interact; this alters the growth and decay of the modes. However, the trend is certainly consistent with the stretching process.

e. Ro = 5.0 and Fr = 0.1

The last parameter choice that we consider is for very large Rossby numbers. We do not claim that this is relevant to many flows of oceanic interest. However, we present it on the basis that it produces a large $\Delta\eta$ while still maintaining small Froude numbers. Interestingly, we find that this produces similar asymmetries as in the previous example.

We present simulations from the Gaussian profile since it produced more dramatic results in comparison to the Bickley jet. The difference is that the Gaussian profile is steeper and therefore relatively more unstable and manages to inject strong cyclones into the deep waters. This was observed in the case of the Bickley jet but only for larger Rossby number.

In Fig. 10 the anticyclonic fluid forms both inner and outer pools where the inner pools pinch off and are injected into the shallow region. The cyclonic fluid generates inner pools that are first elongated and then settle into a triangular vortex with feetlike extensions. These triangular cyclones have been previously observed in both Flierl et al. (1987) and Arai and Yamagata (1994) and are the barotropic versions of the boomerang-shaped objects observed in Fig. 8.

As the instability develops in Fig. 10, the cyclones form triangular shapes and the anticyclones remain elliptical. The vortex street as a whole is advected toward deeper waters. This strengthens the cyclones, which enables them to inject a significant portion of their mass through the street. This forms very strong and concentrated cyclones in the deep water. When the cyclones first separate, they are accompanied by much weaker anticyclones in a dipole. However, the anticyclonic fluid detaches and reenters the street to be stretched out eventually as filaments. We note that there is much wave activity on the edge of the cyclonic vortices in Figs. 10b, 10e, and 10f, which probably results from supersonic instabilities since Ripa's second criteria is violated in this case.

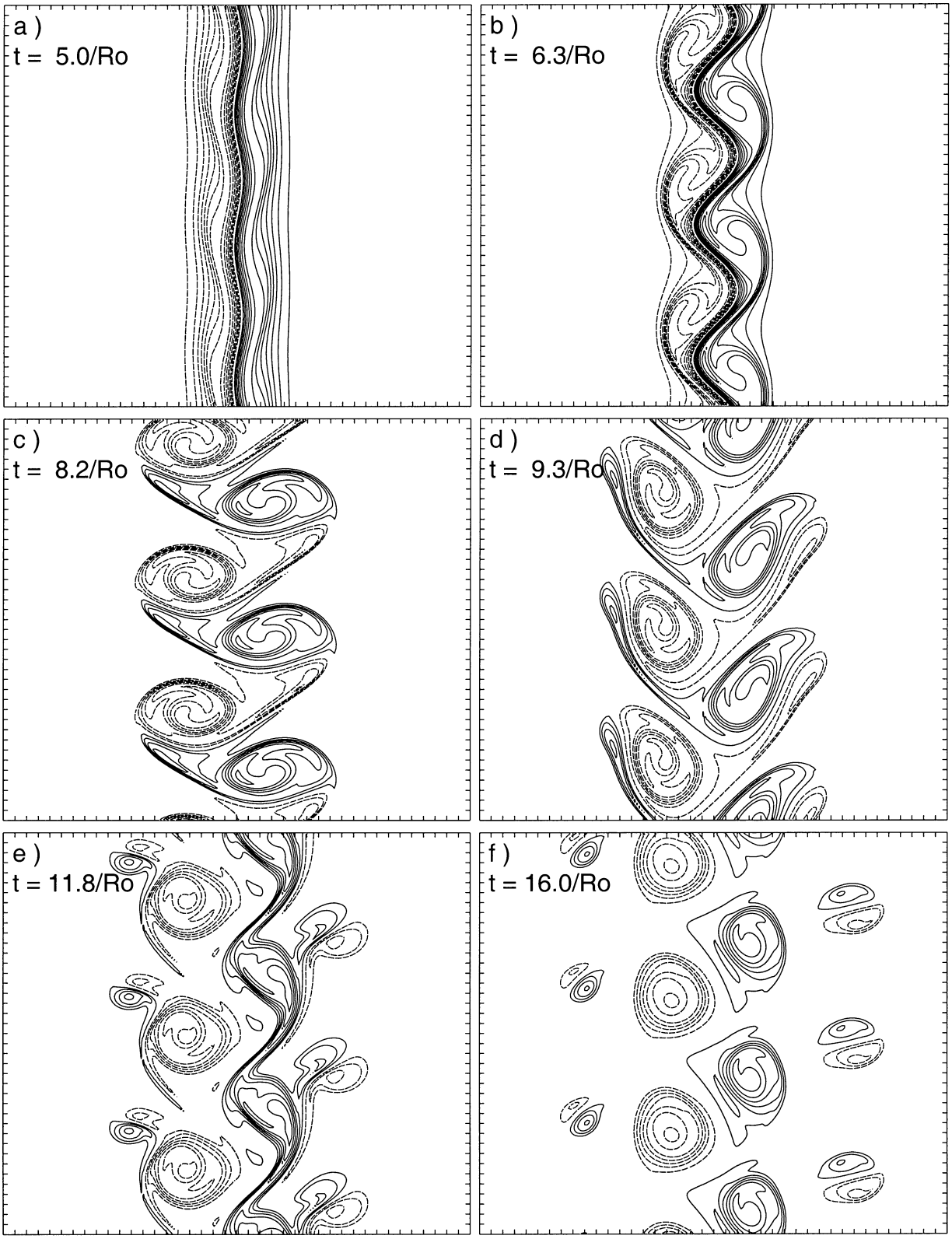

FIG. 7. Case for Ro = 1.0 and Fr = 0.1: asymmetry in the shape of vortices is apparent.

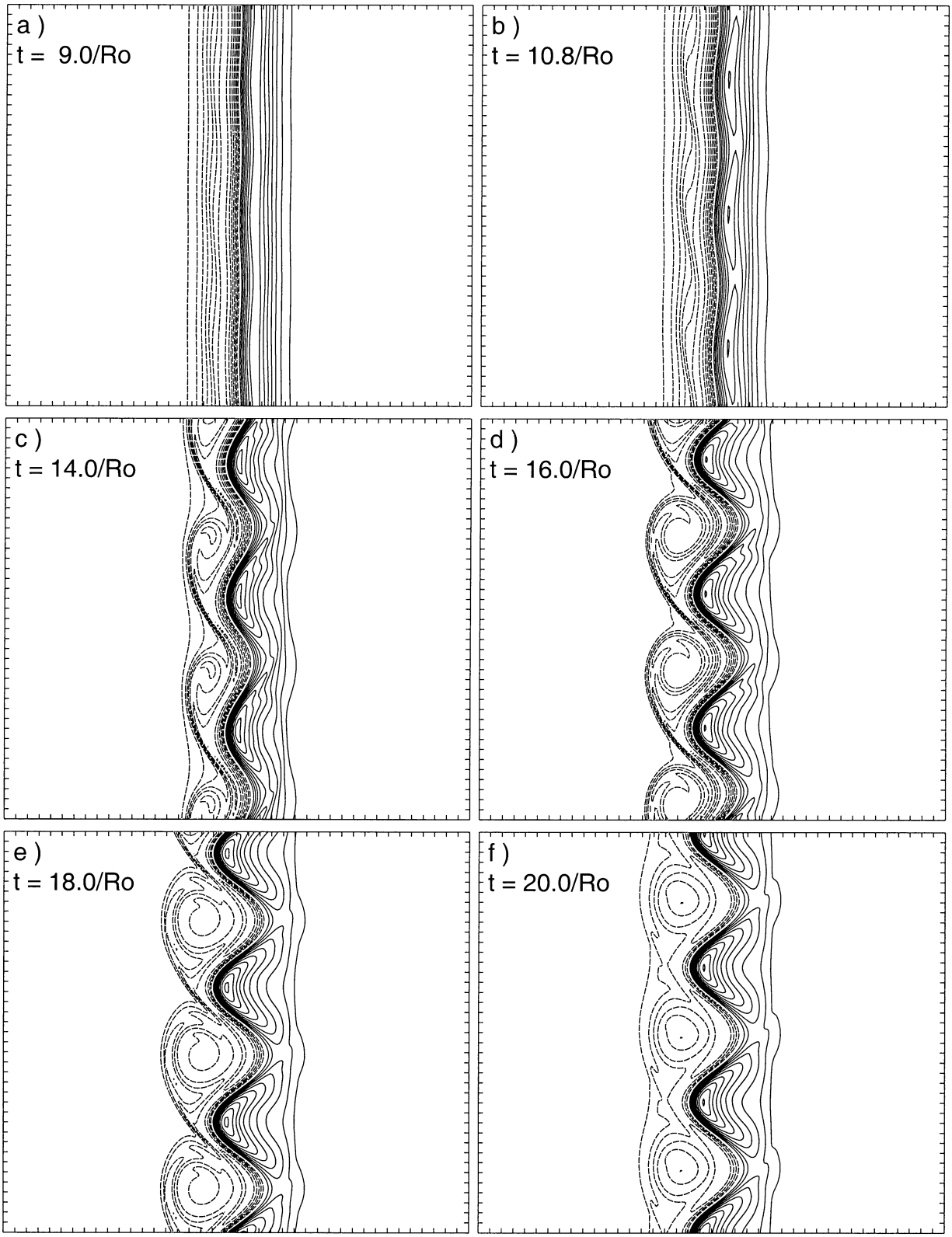

FIG. 8. Case for Ro = 1.0 and Fr = 0.5: in this region of non-QG parameters, the cyclones are stronger and boomerang shaped.

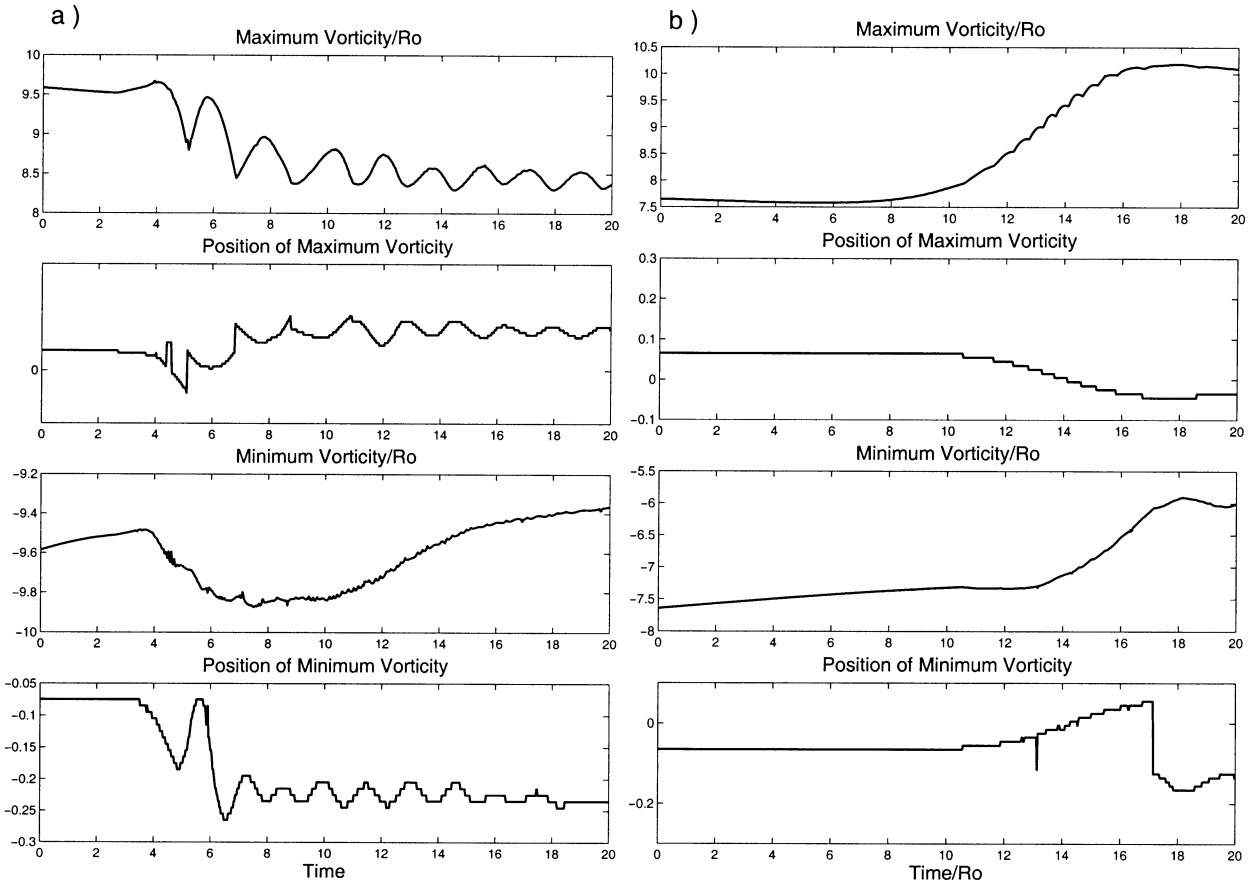

FIG. 9. Case for Ro = 1.0 and (a) Fr = 0.1 and (b) Fr = 0.5: the former and latter are examples in which the anticyclones and cyclones, respectively, are stronger; (b) illustrates that the cyclones become boomerang shaped.

This particular example is important because it illustrates how a strong unstable jet can transport fluid across itself to form coherent cyclones that can then travel for a long period of time and long distances while gradually depositing their contents along the way. This is a means by which mixing can occur on large scales. The properties to be mixed can be chemical, biological, or physical. This process is believed to be an important component of the thermohaline circulation (Flierl and Meid 1985; Wunsch 1984).

f. Polychromatic perturbations

In order to consider more realistic perturbations we present the results from two sets of polychromatic perturbations. We perturb the basic state with the first six along-channel modes, each mode is of the same amplitude. The parameters chosen correspond to those in Figs. 7 and 8, respectively. We present simulations in which the velocity of the basic state is a Gaussian since it illustrates that the initial development is the same as what we saw in the monochromatic Bickley jet profiles.

The first observation from Fig. 11 is that it confirms the prediction from linear theory that $k = 3\pi$ is the most unstable mode. Second, the vortex street is unstable to subharmonics that cause it to break up and form solitary vortices or dipoles. Third, the anticyclones are stronger than the cyclones, as predicted from the monochromatic simulation. This is, of course, the most important finding since it suggests that this qualitative behavior, of anticyclones being stronger, should apply to most jets in this region of parameter space.

We note that, as in the monochromatic case, the polychromatic simulations also eject dipoles away from the unstable street in both directions. Figure 11d clearly indicates that the cyclonic component of the dipoles moving toward deeper waters are stronger than the anticyclones. They do not last very long because of the interaction with the other vortices. The three-dimensional numerical experiments of the SGO in Jungclaus (1999) observed similar asymmetric dipoles ejected into deeper waters. This appears to be a generic feature for highly unstable jets.

The emergence of six vortices in Fig. 12 proves that $k = 3\pi$ is the most unstable mode. The evolution of the instability is as in Fig. 8 except that all of the cyclones (anticyclones) differ in strength because there is more than one unstable mode that is growing. The

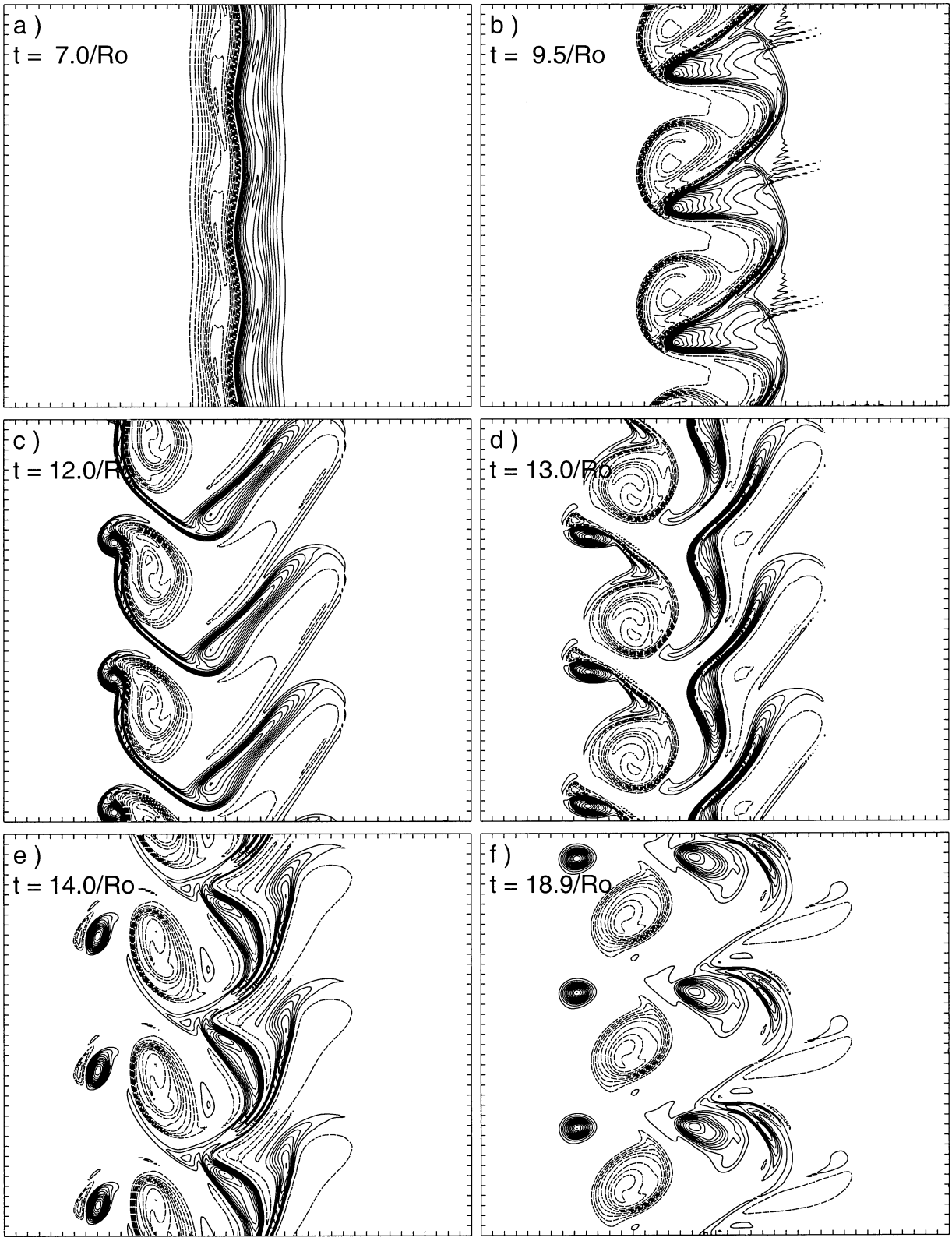

FIG. 10. Case for Ro = 5.0 and Fr = 0.1: in the case of large free-surface deformations and small Froude number, the cyclones become triangular in shape.

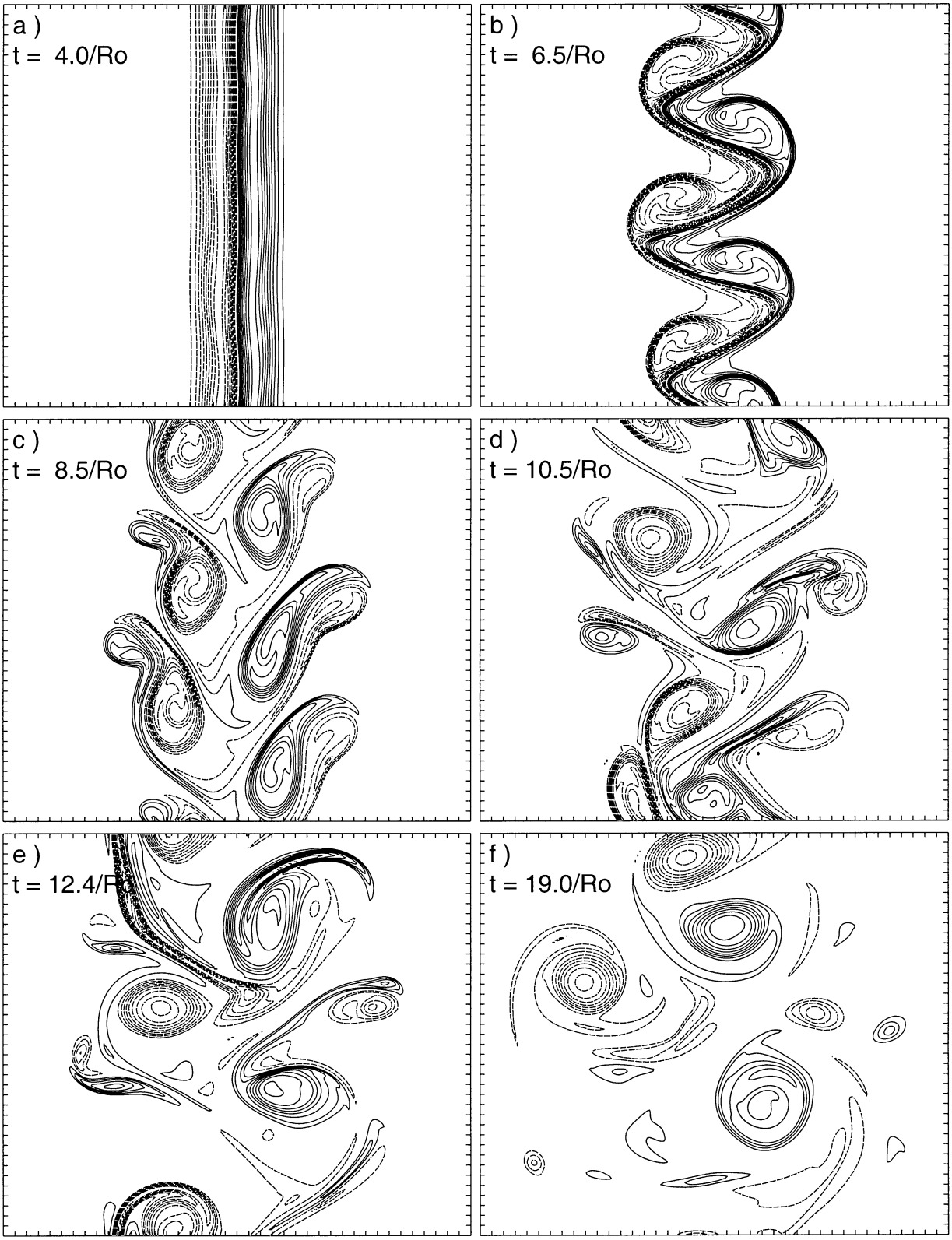

FIG. 11. Case for Ro = 1.0 and Fr = 0.1: a vortex street emerges in asymmetric form.

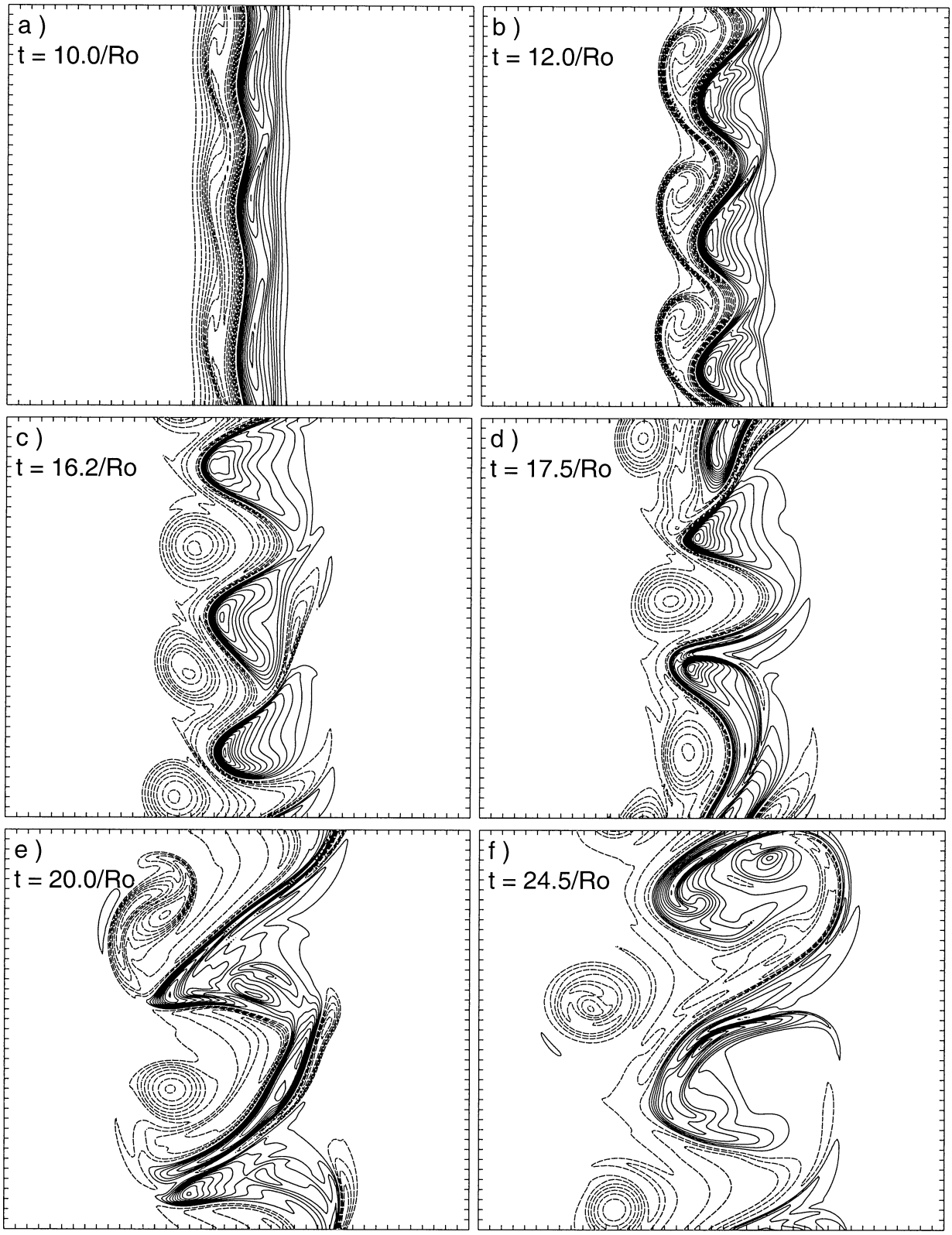

FIG. 12. Case for Ro = 1.0 and Fr = 0.5: a vortex street emerges in highly asymmetric form.

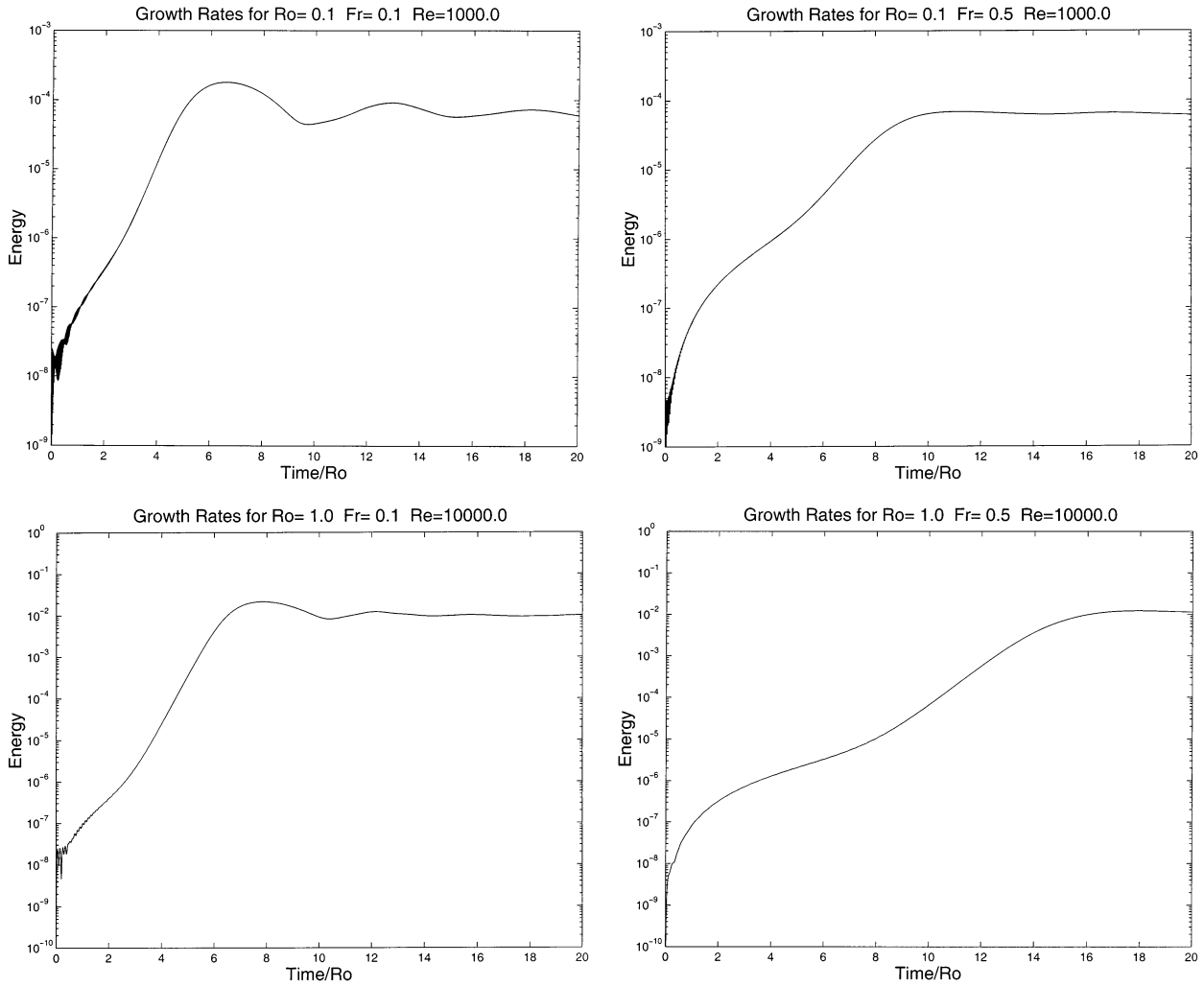

FIG. 13. The logarithm of the growth rates for various Rossby and Froude numbers. Each curve initially levels out to a linear curve, the slope of which yields the growth rate.

growth of subharmonic instabilities causes the merger to take place [see Saffman and Schatzman (1981)]. The merger occurs because the mode-3 vortex street is unstable to perturbations in mode 2. The end state is a vortex street with two sets of cyclones and anticyclones with vortices that are asymmetric in size, strength, and shape.

Both of these polychromatic runs show that the anticyclonic eddies that form tend to be circular in shape. The cyclones that form in Fig. 11 tended to be elliptical whereas those in Fig. 12 are more elongated, like filaments. These two runs demonstrate that the structures that arise in monochromatic runs also arise in polychromatic runs.

5. Growth rates

If we substitute (16) into the integral for the total kinetic energy and exclude the kinetic energy of the geostrophic state, we find that the perturbation kinetic energy is the sum of the following three integrals:

$$\int_{-1}^{+1}\int_{-1}^{+1} \overline{h}\overline{v}v' + \frac{1}{2}\overline{v}^2h'\,dx\,dy \tag{22}$$

$$\int_{-1}^{+1}\int_{-1}^{+1} \overline{v}v'h' + \frac{1}{2}\overline{h}(u'^2 + v'^2) + \frac{1}{2}h'(u'^2 + v'^2)\,dx\,dy \tag{23}$$

$$\int_{-1}^{+1}\int_{-1}^{+1} \frac{1}{2}h'(u'^2 + v'^2)\,dx\,dy. \tag{24}$$

If the perturbations are small, the motion is governed by the linear dynamics and the solution can be decomposed into a sum of normal modes (20). This decomposition implies that the integral of any field, linear or cubic in the perturbation variables, is identically zero.

TABLE 1. A summary of the results from the numerical simulations of the instability of a geostrophic Bickley jet over a flat bottom.

Run	Fr	Ro	$\Delta\eta$	σ_{num}/Ro	σ_{lin}/Ro	Type
1	0.1	0.1	0.01	1.04	1.43	Mono
2	0.1	0.2	0.02	1.22	1.41	Mono
3	0.1	1.0	0.1	1.31	1.41	Mono
4	0.1	5.0	0.5	0.86	0.95	Mono
5	0.1	5.0	0.5	0.84	0.95	Poly
6	0.1	8.0	0.8	0.60	0.68	Mono
7	0.5	0.1	0.05	0.61	0.8	Mono
8	0.5	0.2	0.1	0.72	0.87	Poly
9	0.5	1.0	0.5	0.58	0.61	Mono
10	0.5	1.0	0.5	0.54	0.61	Poly
11	0.5	1.6	0.5	0.50	0.43	Mono

When the linear theory breaks down, this result will no longer be true since the decomposition of modes is no longer possible. Therefore, we chose the quadratic term (23) as the measure of the growth rate since it contains terms that do not vanish in the linear regime (Hayashi and Young 1987). The calculations of the logarithm of the perturbation kinetic energy terms are shown in Fig. 13.

From these plots it is straightforward to calculate the lines that best fit the curves of exponential growth. The slopes of these lines give the growth rates of the nonlinear simulations, the results of which are presented in Table 1. The values obtained from the numerical simulations are within 20% of the theoretical predictions except for the cases in which the Rossby number is 0.1.

In all four cases of Fig. 13 the initial curve is slightly oscillatory but, soon after, becomes a smooth curve that is nearly linear. The straightness of these lines supports the hypothesis that there is exponential growth. The closeness of the growth-rate calculations, combined with the linearity of the curve, strongly suggests that linear growth is indeed the mechanism that dominates the initial stage of the instability.

One source of discrepancy in the two growth rates is diffusion. The linear calculation is done for an inviscid system whereas the nonlinear simulations are only nearly inviscid. This implies that the growth rates for the nonlinear experiments should be less than the predicted values; this is indeed the case for all but one simulation. The experiments with small Rossby number have a smaller numerical Reynolds number for the same value of ν, which is why these simulations have the greatest discrepancies with the linear theory.

Another source of error is that the system is not truly linear. The small nonlinear terms can affect the growth rate by introducing other waves into the system. The presence of multiple modes alters the growth since the additional modes grow at a different rate and hence change the overall growth of the system. This conjecture is supported by our polychromatic perturbations that consistently yield growth rates smaller than their monochromatic equivalents.

6. Summary and conclusions

We have studied the formation of vortices through the barotropic instability of a geostrophic jet in the context of the SW model. The growth of the instability is well described by linear theory. Both the linear and nonlinear theory demonstrated that an increasing Froude number stabilized the flow and an increasing Rossby number created flows that were relatively more stable. Stabilization of the jet is important since it may prevent transport across the jet. Because transportation and decay of eddies play a role in the oceans' thermohaline circulation, this is an important problem of real physical significance. We have not yet quantified the amount of fluid transport or determined how this quantity depends on the two nondimensional parameters. Doing such calculations would also help to identify the regions where the jet acts as a transport barrier. This, of course, has an important impact on biological communities that may be depending on these eddies to transport nutrients.

As expected, the nonlinear simulations for the case of small Rossby number generated the same structures as those that arose in QG theory. We ventured into the non-QG regime to observe the cyclone–anticyclone asymmetries in eddy generation. The anticyclones were always circular in shape and were larger than the cyclones. We found a regime of moderate values of $\Delta\eta$ where anticyclones were the strongest vortex in both the monochromatic and polychromatic simulations. Then for larger values of this parameter, whether it is due to large Rossby number or large Froude number, cyclones are the strongest vortex because of cyclogenesis. In this case the cyclones were sometimes observed to be triangular in shape or filamented. The strong deformation of the cyclones must be due to the fact that they exist in very shallow waters.

We have observed that the case of large $\Delta\eta$ generates stronger cyclones through the injection of cyclonic fluid into deep waters whereby they are then stretched. This is essentially the same mechanism that is believed to cause the vortex asymmetry in the DSO (Spall and Price 1998; Jungclaus et al. 2001). Even though our model is much simpler than this dense water overflow, we observe that even the simple SW model can reproduce this same qualitative behavior without the need for an active upper layer. It would be of interest to proceed with this comparison by analyzing a 2-layer SW model in order to describe baroclinic effects, something we have omitted.

In a following paper we will study the instability of a jet overlying a smooth shelf (F. Poulin and G. Flierl 2003, unpublished manuscript). There, we will investigate how the instability is affected by changes in magnitude, direction, and width of the topography. This will have implications for coastal problems where the flow is along the shelf.

Acknowledgments. This work was supported by NSF Grant 6890413.

REFERENCES

Allen, J. S., J. A. Barth, and P. A. Newberger, 1990a: On intermediate models for barotropic continental shelf and slope flow fields. Part I: Formation and comparison of exact solutions. *J. Phys. Oceanogr.,* **20,** 1017–1042.

——, ——, and ——, 1990b: On intermediate models for barotropic continental shelf and slope flow fields. Part III: Comparison of numerical model solutions in periodic channels. *J. Phys. Oceanogr.,* **20,** 1949–1973.

Arai, M., and T. Yamagata, 1994: Asymmetric evolution of eddies in rotating shallow water. *Chaos,* **4,** 163–175.

Armi, L., and W. Zenk, 1984: Large lenses of highly saline mediterranean water. *J. Phys. Oceanogr.,* **14,** 1560–1576.

Baey, J.-M., P. Riviere, and X. Carton, 1999: Ocean jet instability: A model comparison. *Proc. of the Third IWVF,* Toulouse, France, ESAIM, 12–23.

Balmforth, N. J., 1999: Shear instability in shallow water. *J. Fluid Mech.,* **387,** 97–127.

Barth, J. A., J. S. Allen, and P. A. Newberger, 1990: On intermediate models for barotropic continental shelf and slope flow fields. Part II: Comparison of numerical model solutions in doubly periodic domains. *J. Phys. Oceanogr.,* **20,** 1044–1076.

Drazin, P. G., and W. H. Reid, 1995: *Hydrodynamic Stability.* Cambridge University Press, 527 pp.

Fletcher, C. A. J., 1991: *Computational Techniques for Fluid Dynamics.* Springer-Verlag, 1024 pp.

Flierl, G. R., and R. P. Meid, 1985: Frictionally induced circulations and spin down of a warm-core ring. *J. Geophys. Res.,* **90,** 8917–8927.

——, P. Malanotte-Rizzoli, and N. J. Zabusky, 1987: Nonlinear waves and coherent vortex structures in barotrophic β-plane jets. *J. Phys. Oceanogr.,* **17,** 1408–1438.

——, X. Carton, and C. Messager, 1999: Vortex formation by unstable oceanic jets. *Proc. of the Third IWVF,* Toulouse, France, ESAIM, 137–150.

Hayashi, Y.-Y., and W. Young, 1987: Stable and unstable shear modes of rotating parallel flows in shallow water. *J. Fluid Mech.,* **184,** 477–504.

Holton, J. R., 1992: *An Introduction to Dynamic Meteorology.* Academic Press, 511 pp.

Jungclaus, J. H., 1999: A three-dimensional simulation of the formation of anticyclonic lenses (meddies) by the instability of an intermediate depth boundary current. *J. Phys. Oceangr.,* **29,** 1579–1598.

——, J. Hauser, and R. H. Käse, 2001: Cyclogenesis in the Denmark Strait overflow plume. *J. Phys. Oceanogr.,* **31,** 3214–3229.

Karsten, R. H., G. E. Swaters, and R. E. Thomson, 1995: Stability characteristics of deep-water replacement in the Strait of Georgia. *J. Phys. Oceanogr.,* **25,** 2391–2403.

Lane-Serff, G. F., and P. G. Baines, 1998: Eddy formation by dense flows on slopes in rotating fluid. *J. Fluid Mech.,* **363,** 229–252.

Li, S., and T. A. McClimans, 2000: On the stability of barotropic prograde and retrograde jets along a bottom slope. *J. Geophys. Res.,* **105,** 8847–8855.

McWilliams, J. C., 1985: Submesoscale, coherent vortices in the ocean. *Rev. Geophys.,* **23,** 165–182.

Olson, D. B., 1991: Rings in the ocean. *Annu. Rev. Earth Planet. Sci.,* **19,** 283–311.

Paldor, N., and M. Ghil, 1997: Linear instability of a zonal jet on an f plane. *J. Phys. Oceanogr.,* **27,** 2361–2369.

Pedlosky, J., 1987: *Geophysical Fluid Dynamics.* Springer-Verlag, 710 pp.

——, 1996: *Ocean Circulation Theory.* Springer-Verlag, 453 pp.

Polvani, L. M., J. C. McWilliams, M. A. Spall, and R. Ford, 1994: The coherent structures of shallow-water turbulence: Deformation-radius effects, cyclone/anticyclone asymmetry and gravity-wave generation. *Chaos,* **4,** 177–186.

Poulin, F. J., and G. E. Swaters, 1999a: Sub-inertial dynamics of density-driven flows in a continuously stratified fluid on a sloping bottom. Part I: Model derivation and stability characteristics. *Proc. Roy. Soc. London,* **445A,** 2281–2304.

——, and ——, 1999b: Sub-inertial dynamics of density-driven flows in a continuously stratified fluid on a sloping bottom. Part II: Isolated eddies and radiating cold domes. *Proc. Roy. Soc. London,* **445A,** 2305–2329.

Prater, M. D., and T. B. Sanford, 1994: A meddy off cape St. Vincent. Part I: Descrition. *J. Phys. Oceanogr.,* **24,** 1572–1586.

Reszka, M. K., G. E. Swaters, and B. R. Sutherland, 2002: Instability of abyssal currents in a continuously stratified ocean with bottom topography. *J. Phys. Oceanogr.,* **32,** 3528–3550.

Ripa, P., 1983: General stability conditions for zonal flows in a one-layer model on the β-plane or the sphere. *J. Fluid Mech.,* **126,** 463–489.

——, 1991: General stability conditions for a multi-layer model. *J. Fluid Mech.,* **222,** 119–137.

Rogerson, A. M., P. D. Miller, L. J. Pratt, and C. K. R. T. Jones, 1999: Lagrangian motion and fluid exchange in a barotropic meandering jet. *J. Phys. Oceangr.,* **29,** 2635–2655.

Saffman, P. G., and J. C. Schatzman, 1981: Properties of a vortex street of finite vorticies. *SIAM J. Sci. Stat. Comut.,* **2,** 285–295.

Schär, C., and H. C. Davies, 1990: An instability of mature cold fronts. *J. Atmos. Sci.,* **47,** 929–950.

Spall, M. A., and J. F. Price, 1998: Mesoscale variability in Denmark Strait: The PV outflow hypothesis. *J. Phys. Oceanogr.,* **28,** 1598–1623.

Stegner, A., and D. G. Dritschel, 2000: A numerical investigation of the stability of isolated shallow water vortices. *J. Phys. Oceanogr.,* **30,** 2562–2573.

Swaters, G. E., 1991: On the baroclinic instability of cold-core coupled density fronts on a sloping continental shelf. *J. Fluid Mech.,* **224,** 361–382.

——, and G. R. Flierl, 1991: Dynamics of ventilated coherent cold eddies on a sloping bottom. *J. Fluid Mech.,* **223,** 565–588.

Takehiro, S.-I., and Y.-Y. Hayashi, 1992: Over-reflection and shear instability in a shallow-water model. *J. Fluid Mech.,* **236,** 259–279.

Trefethen, L. N., 2000: *Spectral Methods in Matlab.* SIAM, 165 pp.

Vallis, G. K., 1996: Potential vorticity inversion and balanced equations of motion for rotating and stratified flows. *Quart. J. Roy. Meteor. Soc.,* **122,** 291–322.

Wunsch, C., 1984: The ocean circulation in climate. *The Global Climate,* J. T. Houghton, Ed., Cambridge University Press, 189–203.